Adding Proximity Sensing Capability to Tactile Array Based on Off-the-Shelf FSR and PSoC

Julián Castellanos-Ramos, Andrés Trujillo-León, Rafael Navas-González, Francisco Barbero-Recio, José Antonio Sánchez-Durán, Óscar Oballe-Peinado, and Fernando Vidal-Verdú

***Abstract*— Tactile sensors have been incorporated into robots to help in many tasks, such as preventing damage to humans in collaborative works or assistance or in dexterous manipulation. Proximity sensors are also common in robotics and are proposed to implement pretouch in multimodal realizations. Many tactile sensors are based on off-the-shelf force-sensing resistors (FSRs). The parasitic capacitance associated with the electrodes of the FSR can be exploited to measure proximity. Moreover, it is possible to implement both force and proximity signal acquisition with a single chip. This article presents a multimodal proximity and tactile patch based on commercial FSR plus a programmable system on chip (PSoC). The ability to measure proximity is achieved without adding any extra element. Discussions about key design issues as well as results that show the performance of the sensor patch are presented. As proximity sensing array, the range is in the order of the size of the electrodes, and it depends on the properties of the object nearby, as expected. The best performance is observed for conductive objects. Therefore, this approach is especially interesting in human–robot interaction tasks, such as shaping robotic hands or grippers around the human body. Furthermore, dielectric objects are also detected, so it can also be used to implement pretouch in manipulation tasks.**

***Index Terms*— Multimodal sensors, pretouch, programmable system on chip (PSoC), proximity sensors, tactile sensors.**

I. Introduction

PROXIMITY sensors are used to avoid collision in robotics. Sensitive skins that integrate many proximity sensors have been proposed in human–robot cooperation or assistive robotics to prevent damage to humans or objects [1], [2]. Tactile sensors are also aimed at achieving the same goal, but the need to establish contact to detect objects means a cautious and somewhat slow operation of the robot. A multimodal approach is proposed by many authors where proximity sensing is exploited to detect the objects before making contact. This so-called "pretouch" is also implemented to shape the fingers in robotic hands or grippers before physical contact with the objects or human beings is established (pregrasp [3], [4]). Moreover, this also called "proximity servoing" [5] complements the large-range visual servoing where occlusion is common at short distance in manipulative tasks. Proximity servoing allows a much more efficient manipulation because it can be more fluent without knocking or moving the object out of the working range of the hand or gripper [4]. Moreover, the pose of the fingers can be preadjusted, so the grasp is more stable once it is made. This servoing also allows the robot and human hands to be aligned in cooperation tasks [6], [7].

Proximity sensors are commonly capacitive or optical. Pairs of LEDs and phototransistors are frequently used to implement optical proximity sensors [3], [8]. They are accurate, but their response depends on features such as surface reflectivity and color, or ambient light if they are based on triangulation. Moreover, they cannot properly detect transparent or very reflective metallic objects. In addition, the response can be nonmonotonic, so further smart processing is required. Cameras have also been used to implement proximity sensing, as auxiliary devices to calibrate LED-phototransistor-based sensors [9], or as stand-alone devices mounted on the fingers [10], or using special setups [11]. Other optical sensors are based on time of flight (ToF) [12] or on the ratio between the reflected intensity of two modulated signals and their phase [13]. The response of these sensors does not depend on the surface reflectivity of the object. Optical sensors can also have a relatively large minimum distance detection (in the order of 1 cm). This is not the case with the one reported in [13] that shows high performance in terms of range and resolution, though it is not an array, but a single sensor mounted at the tip of a gripper, and it is relatively large and complex compared with a basic capacitive proximity sensor. On the other hand, capacitive proximity sensors are simple and have low cost. However, their output is affected by electrical fields in the environment. In addition, the output depends on the conductive nature of the object. Metals or highly conductive objects are well detected, while the response to dielectric material depends on their properties [14].

Once the contact is made, tactile sensors can provide essential information to achieve dexterous manipulation [15]. A number of authors propose multimodal solutions that implement different sensors to increase the proprioceptive capabilities of the robot, and, specifically, tactile and proximity

Manuscript received February 12, 2019; revised September 10, 2019; accepted September 16, 2019. Date of publication September 30, 2019; date of current version June 9, 2020. This work was supported in part by the Spanish Government and in part by the European ERDF Program Funds under Contract TEC2015-67642-R. The Associate Editor coordinating the review process was Bruno Ando. *(Corresponding author: Julián Castellanos-Ramos.)*

J. Castellanos-Ramos, R. Navas-González, J. A. Sánchez-Durán, Ó. Oballe-Peinado, and F. Vidal-Verdú are with the Departamento de Electrónica, Universidad de Málaga, 29071 Málaga, Spain, and also with the Instituto de Investigación Biomédica de Málaga (IBIMA), 29010 Málaga, Spain (e-mail: jcramos@uma.es).

A. Trujillo-León is with the Institute for Intelligent Systems and Robotics (ISIR), Sorbonne University, 75005 Paris, France.

F. Barbero-Recio is with the TDK Group, 28906 Madrid, Spain.

Color versions of one or more of the figures in this article are available online at http://ieeexplore.ieee.org.

Digital Object Identifier 10.1109/TIM.2019.2944555

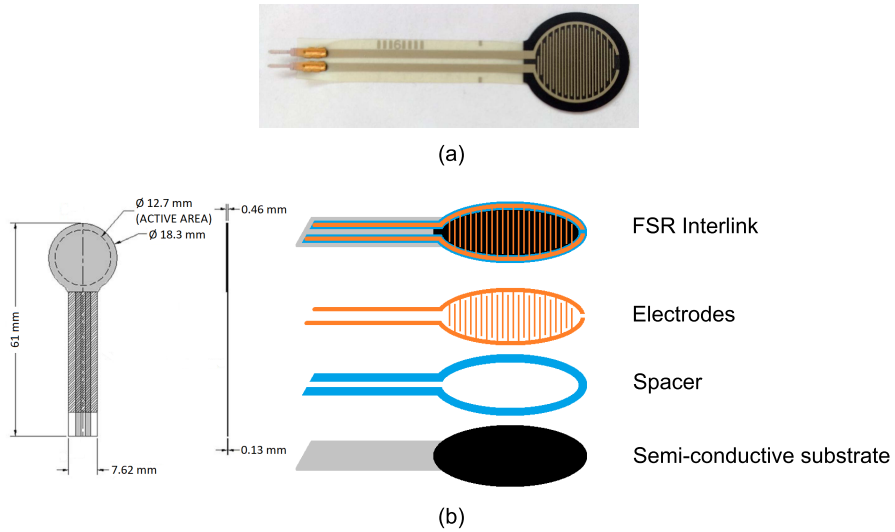

Fig. 1. (a) Photograph of an FSR from interlink and (b) components and dimensions.

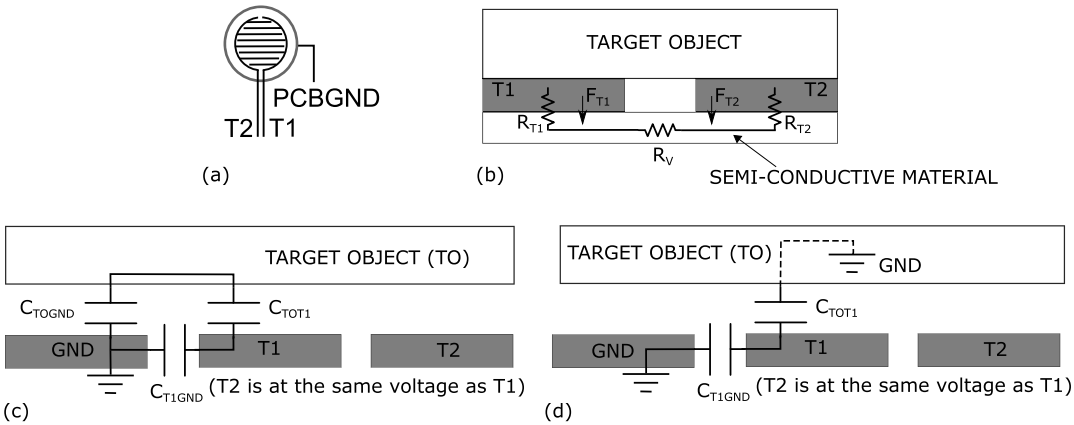

Fig. 2. Basic models of the device. (a) Symbol. (b) Model as a force sensor. (c) Model as proximity sensor with a dielectric TO. (d) Model as proximity sensor with a highly conductive object.

sensors. For instance, an optical proximity sensor is embedded in an elastomer that acts as a spring and allows force measurements, while proximity is sensing beyond the elastomer outer surface [3]. Similar approaches have been followed to achieve both the tactile and the proximity sensing in capacitive sensors [16], [17], while other sophisticated skins incorporate more sensors [14]. Another multimodal sensor based on a 3-D microstructure is reported in [18], where proximity is detected by capacitive transduction.

This article presents a multimodal tactile and proximity sensor based on off-the-shelf devices. The proposed approach can be used to extend the capabilities of tactile sensors built with force-sensing resistors (FSRs), such as those in [19] and [20]. When compared with other mentioned multimodal realizations, the device does not add a proximity sensor, but it takes advantage of the electrodes of the FSR to implement capacitive proximity sensing. Second, a design based on a programmable system on chip (PSoC) [21] is proposed. This device allows the configuration of the hardware, as field-programmable gate arrays (FPGAs) do. However, although the digital aspect is much less complex and powerful than that of FPGA, it has also configurable analog hardware. Moreover, it allows dynamic configuration of the internal circuitry at execution time. This capability is exploited to implement both the tactile and the proximity signal conditioning circuitry on the same chip and switch between them to detect proximity and contact force. In this way, the proposal achieves a very compact design whose electronics is in a single chip.

II. Materials and Methods

A. Off-the-Shelf Force-Sensing Resistor and Use as Proximity Sensor

An FSR from Intelink Electronics [22] was selected to illustrate the approach and build the prototype. Table I summarizes its main characteristics. A tactile sensor patch for a robotic arm based on these sensors was reported by Vidal-Verdú *et al.* [19]. Similar sensors have been mounted on robotic hands [20]. In both cases, the capabilities of the sensor can be extended to sense proximity besides force.

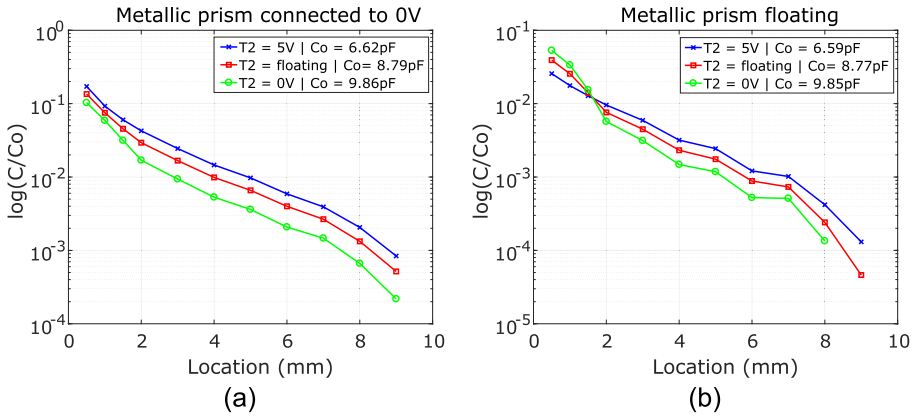

Fig. 3. (a) Change in capacitance with several voltages in terminal 2 of the FSR when the metallic prism is connected to ground and (b) when it is floating.

TABLE I
FSR CHARACTERISTICS

Parameter	Value
Semi-conductive substrate	FSR® carbon-based ink
Electrodes	Silver polymer ink
Dimension of active area	Ø12.7 mm
Sensor thickness	0.46 mm
Force sensitivity range	~ 0.1 to 10 N
Resistance range	~ 1 KΩ to >1 MΩ
EMI / ESD	Generates no EMI; not ESD sensitive

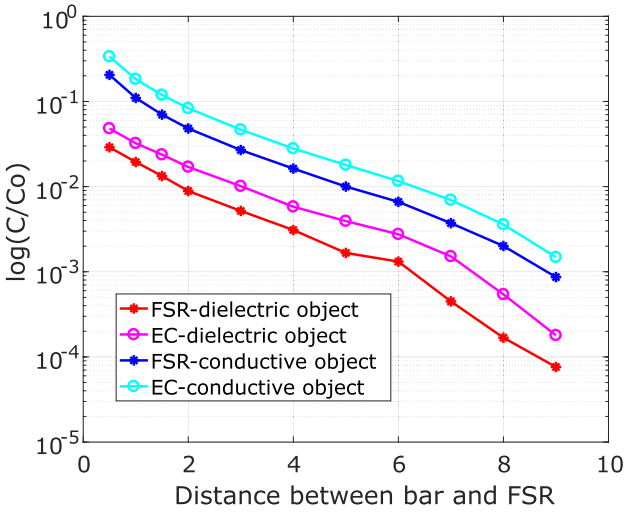

Fig. 4. Simulation results for the device working as proximity sensor (FSR) and one with an EC for conductive as well as dielectric objects approaching the sensor.

Fig. 1(a) shows a photograph of the sensor, and Fig. 1(b) shows a picture of its components and dimensions. Note that it consists of two comb electrodes separated from a conductive material by a thin spacer ring. Beyond a small force threshold,

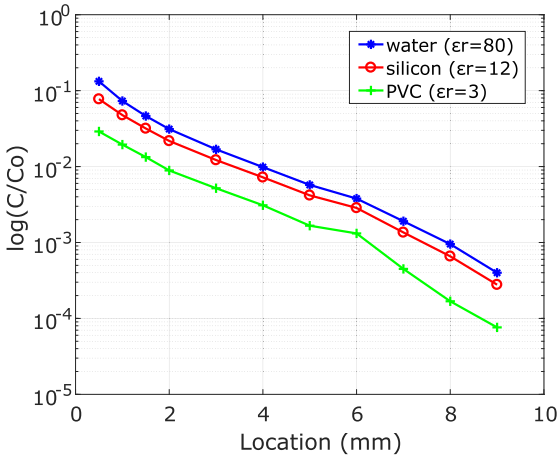

Fig. 5. Simulation results of the device working as proximity sensor and dielectric objects of different permittivity approaching the sensor.

the electrodes make contact with the semiconductive material and the electrical resistance between them varies with the value of the force. This provides a simple way to measure force.

The symbol of the device soldered on the printed circuit board (PCB) is shown in Fig. 2(a). Its model working as a force sensor is shown in Fig. 2(b), where R_{T1} and R_{T2} model the resistance associated with the contact interface and R_V is the resistance of the semiconductive material between the electrodes. There are different working principles behind this sort of resistive force sensors. The FSR used in this article is based on the change in the effective contact area at a microscopic scale. The basic aspects that can help to understand the performance of the device as used for both force sensing and proximity sensing are discussed in the following, while more extensive modeling can be found in [23]. The resistance at the interface of the electrode T_i ($i = 1, 2$ in Fig. 2) is [24]

$$R_{Ti} = \frac{\rho E}{2} \frac{1}{K_{Ti}}$$

where ρ and E are the combined resistivity and elastic modulus of the materials in contact (the electrodes and the semiconductive material) and K_{Ti} is the interfacial stiffness.

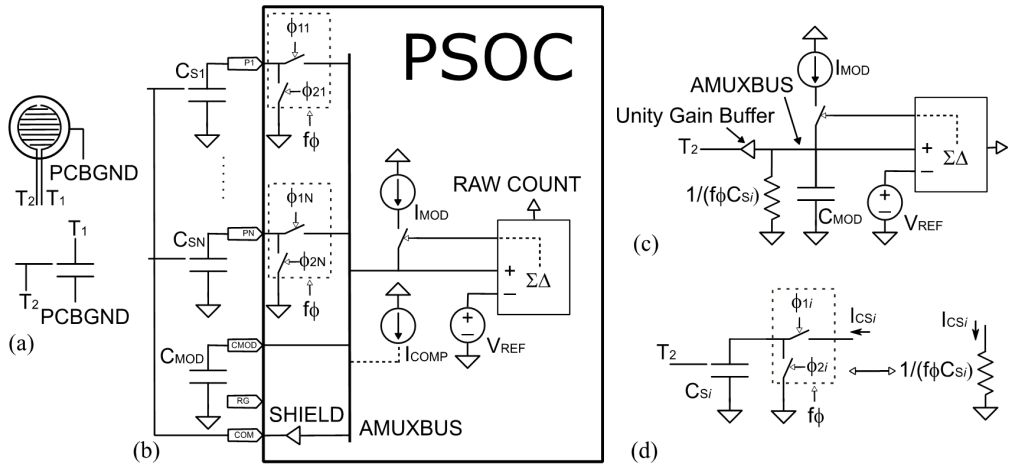

Fig. 6. Configuration to provide the digital output for proximity. (a) Symbol used for the FSR. (b) Connection diagram. (c) Schematic of the circuit when the ith FSR is selected. (d) Resistive model of (e) switched capacitor.

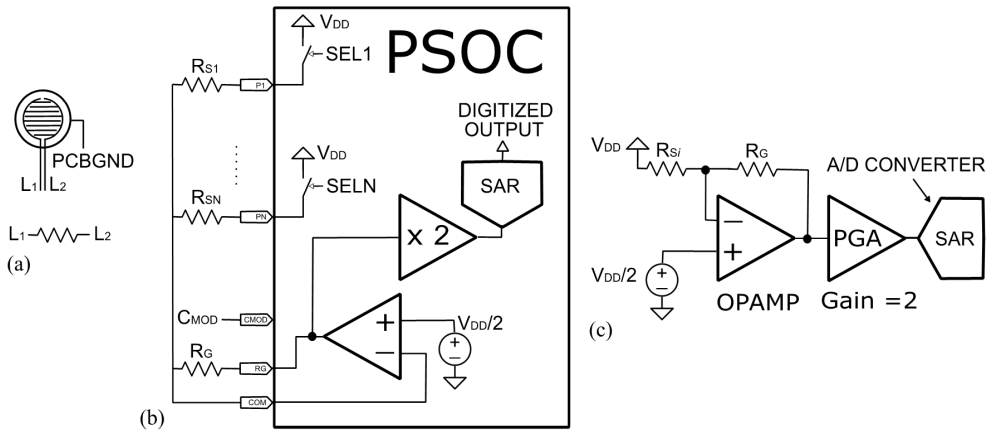

Fig. 7. Configuration to provide the digital output for force. (a) Symbol used for the FSR. (b) Connection diagram. (c) Schematic of the circuit when the ith FSR is selected.

If the statistical distribution of the microcontacts sizes and local pressures remains constant as the load increases, K_{Ti} is linear with the normal force on the contact F_{Ti} [25]. If the force and the contact area in both electrodes are similar, the equivalent resistance that models the sensor is

$$R_S = \frac{k}{F}$$

where F is the force on both contacts, R_V has been neglected, and k is a constant that depends on the contact area and the properties of the materials in contact. Note that there is a linear relationship between the conductance of the sensor ($G_s = 1/R_s$) and the force applied on it. Deviations of this behavior are due to different pressure distributions at the edges of the electrodes and large-wavelength features along the contact interface. It could be argued that a circular electrode (CE) could diminish these undesired effects. However, this means that it is only possible to detect objects of a size similar to the sensor. The use of comb electrodes allows detecting objects smaller than the size of the sensor, of the order of the width of one comb teeth plus the separation between the electrodes.

The aim here is to show that the device in Fig. 1 can also be used to measure proximity. However, the condition of having comb electrodes has to be considered when it is used to implement proximity sensing. The reason is that the distance between the electrodes is small and so the distance range if the capacitance between both electrodes T1 and T2 of the FSR is used for proximity sensing.

Therefore, the capacitance to exploit is that between one of the two electrodes of the sensor (T1) and the ground plane that surrounds the sensor. COMSOL finite-element simulations were performed to observe the influence of the voltage at the other electrode (T2). Fig. 3(a) and (b) shows the simulated change in capacitance between one electrode of the sensor and ground when a metallic piece approaches the sensor. The first electrode (T1) is at 5 V and the metallic piece is grounded in Fig. 3(a), while it is floating in Fig. 3(b). They show three curves that correspond to three situations where the second electrode (T2) of the sensor is floating, grounded, or connected to 5 V. The sensitivity and range of the sensor are better when the second electrode (T2) is also kept at 5 V, i.e., it should be kept at the same voltage

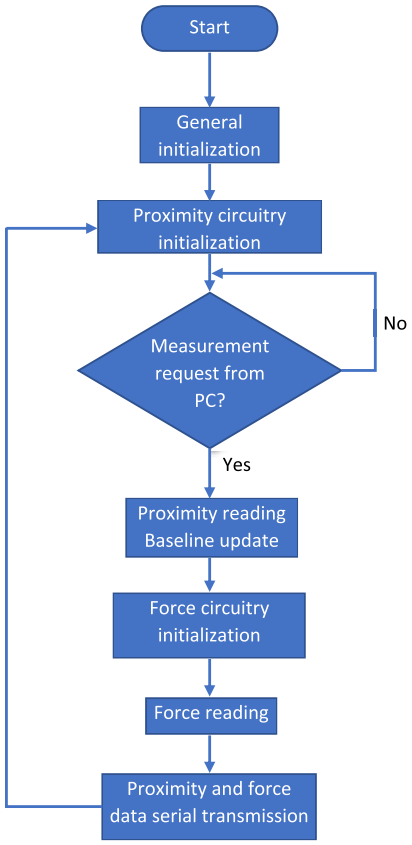

Fig. 8. Flowchart of the basic code in the PSoC to scan the array for proximity and tactile sensing.

as the other electrode (T1). It can be observed in Fig. 3(b) that the sensitivity is higher at short distances (below 2 mm) if the electrode T2 is grounded or floating. This is because the piece crosses the electric field lines between both electrodes. Nevertheless, the range is clearly better if both the electrodes are at the same voltage.

The key issues involved in the performance of a planar capacitor as a proximity sensor are extensively studied in [26], while an analytical method is used in [27] to study the performance of a concentric-ring-shaped sensor for proximity measurement of a grounded metal disk. Based on those in [26], Fig. 2(c) and (d) shows the models of the sensor when the target object (TO) is a dielectric (not grounded) and when it is made of metal, respectively. In the case of a dielectric TO [see Fig. 2(c)], the sensor works in the transmission mode and large electrodes provide better distance and dynamic ranges, and they increase with the separation between the edges of the electrodes. The distance range is in the order of half of the distance between the centers of the electrodes [26].

In the case of a metallic or highly conductive object, the sensor works in single-electrode mode, and the model is that in Fig. 2(d). For a high capacitive coupling between the TO and the ground, the equivalent capacitance is C_{TOT1} and it is described by the equations of a parallel-plate capacitor. Increasing the separation between the electrodes improves the performance, and the distance range, in this case, is of the order of the distance between the centers of the electrodes [26].

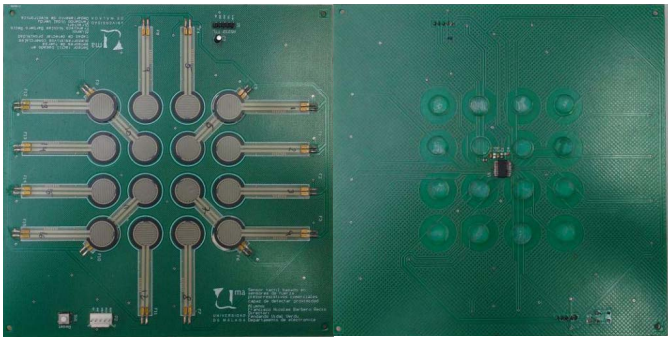

Fig. 9. Prototype of the proximity and tactile patch: top side with the sensors (left) and bottom side with the PSoC (right).

Regarding the influence of the shape of the electrodes, the resulting proximity sensor has a comb-shaped electrode surrounded by a ground plane as a second electrode. COMSOL simulations were carried out to know the influence of this condition. Fig. 4 shows the response of the sensor when a conductive as well as a dielectric object approach the sensor for a CE and for a comb electrode such as that of the FSR. Note that the dynamic range and sensitivity are smaller for the comb electrode than those obtained for the CE. Also note that the distance range (for a given capacitance detection threshold) is smaller for dielectric objects than for conductive objects, which is coherent with the fact commented earlier that the distance range in the transmission mode (for dielectrics) is approximately half of that in single-electrode mode (for conductive objects). Moreover, Fig. 5 shows the response for different representative materials, specifically for PVC ($\varepsilon_r = 3$), silicon ($\varepsilon_r = 12$), and water ($\varepsilon_r = 80$).

Finally, the ground plane that surrounds the sensor also reduces the interferences and helps to concentrate on the electric field related to one sensor in an array and so reduces the crosstalk. However, this ground plane must not be solid, but hatched. Otherwise, the capacitance is substantial when compared to the change produced by a conductive or non-conductive object that is near the sensor. As a consequence, the sensitivity decreases.

B. Proximity and Tactile Signal Conditioning With a Single Integrated Circuit

An off-the-shelf PSoC from Cypress is used to implement both force and proximity sensing signal conditioning. The specific device of this article is the CY8C28445 [21]. The user module "SmartSense2X_EMC" is exploited to measure proximity. It is based on Capsense, a capacitive touch sensing technology from Cypress that uses a sigma–delta converter to perform capacitive-to-digital conversion [28]. Fig. 6(a) and (b) shows the connection diagram. As the array of capacitors is scanned, the selected capacitor is connected and disconnected alternately through the switches at a certain frequency f_ϕ. From a well-known theory on switched-capacitor circuits, the value of the capacitor and the frequency determines the current from the analog bus AMUXBUS as $I_{CSi} = C_{Si} f_\phi V_{\mathrm{AMUXBUS}}$, where C_{Si} is the capacitance between the

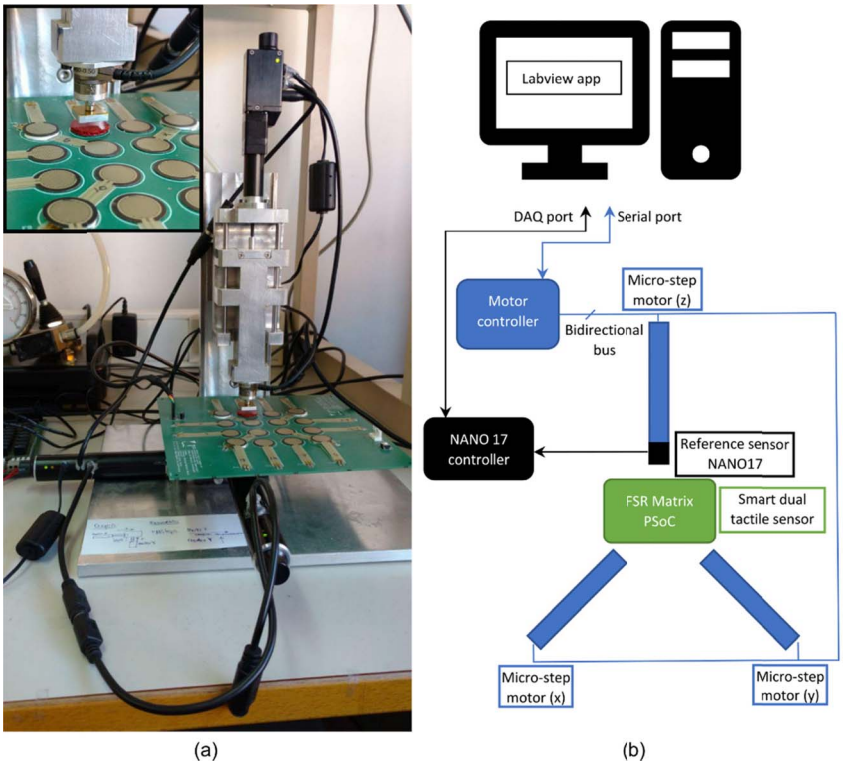

Fig. 10. (a) Photograph and (b) diagram of the experimental setup.

electrode T1 and the ground associated with the ith FSR and V_{AMUXBUS} is the voltage at the analog bus. This can be modeled as shown in Fig. 6(d), while Fig. 6(c) shows the corresponding schematic of the circuitry when the ith sensor is selected. The closed loop with the sigma–delta modulator keeps the voltage at the analog bus V_{AMUXBUS} close to V_{REF}, since both voltages are compared and the modulated output connects and disconnects the current source I_{MOD} to compensate any difference at the input caused by the current demanded by the selected capacitor. This loop determines the converter digital output corresponding to C_{Si}. A second compensation current source I_{COMP} improves the sensitivity. The capacitance C_{Si}, in the absence of an object in the proximity provides an output that is taken as the so-called baseline. When the object approaches the sensor, the output value increases with respect to this baseline. The baseline is updated dynamically to compensate for the changes in the environment. Note that the second electrode (T2) of all the sensors is connected to the same pin (COM in Fig. 6) that follows the voltage at the other electrode (T1), as indicated in Section II-A.

Regarding the signal conditioning as a force sensor, Fig. 7(a) and (b) shows the connection diagram. Note that the external connections that are shared by both configurations in Figs. 6 and 7 are not altered, but the internal connections are changed. Fig. 7(c) shows the schematic of the resulting circuit when one FSR is selected in this mode. This signal conditioning circuitry provides a nearly linear output [22], since the output is proportional to the sensor conductance, which depends linearly on the force (see Section II-A). There is not any user module in the PSoC library to implement an isolated operational amplifier (OPAMP). However, it is possible to configure a continuous-time (CT) analog block in the PSoC to see it as an OPAMP, and both the inverting as well as the output of the OPAMP are accessible from the PSoC pins and can be connected, as shown in Fig. 7(b). The noninverting input is internally connected to a voltage $V_{\mathrm{DD}}/2$. Since the output voltage range of the transimpedance amplifier is $V_{\mathrm{DD}}/2$, a second amplifier with gain 2 is used to obtain a range of V_{DD} at the input of the SAR analog-to-digital converter. To be able to select a specific sensor, the pin driver is configured in the open-drain mode. In this way, it can be seen as a switch that connects the sensor to V_{DD}, as shown in Fig. 7. The sensor is then selected easily by writing the associated port register.

To implement both tactile sensing and proximity sensing, the code in the PSoC scans the array first to detect proximity and second to register the force in every FSR. For that purpose, the code configures the hardware, as shown in Figs. 6 and Fig. 7. A flowchart that represents this code is shown in Fig. 8. Note that both force and proximity readings of one sensor are transmitted through the RS232 serial bus in every iteration, but this can change depending on the specific application. Moreover, the above-mentioned baseline is also updated in every iteration. This makes the reading robust against changes in the environment such as temperature and humidity but introduces a significant drift in the proximity reading. This baseline should be updated more slowly in applications that do not tolerate this drift.

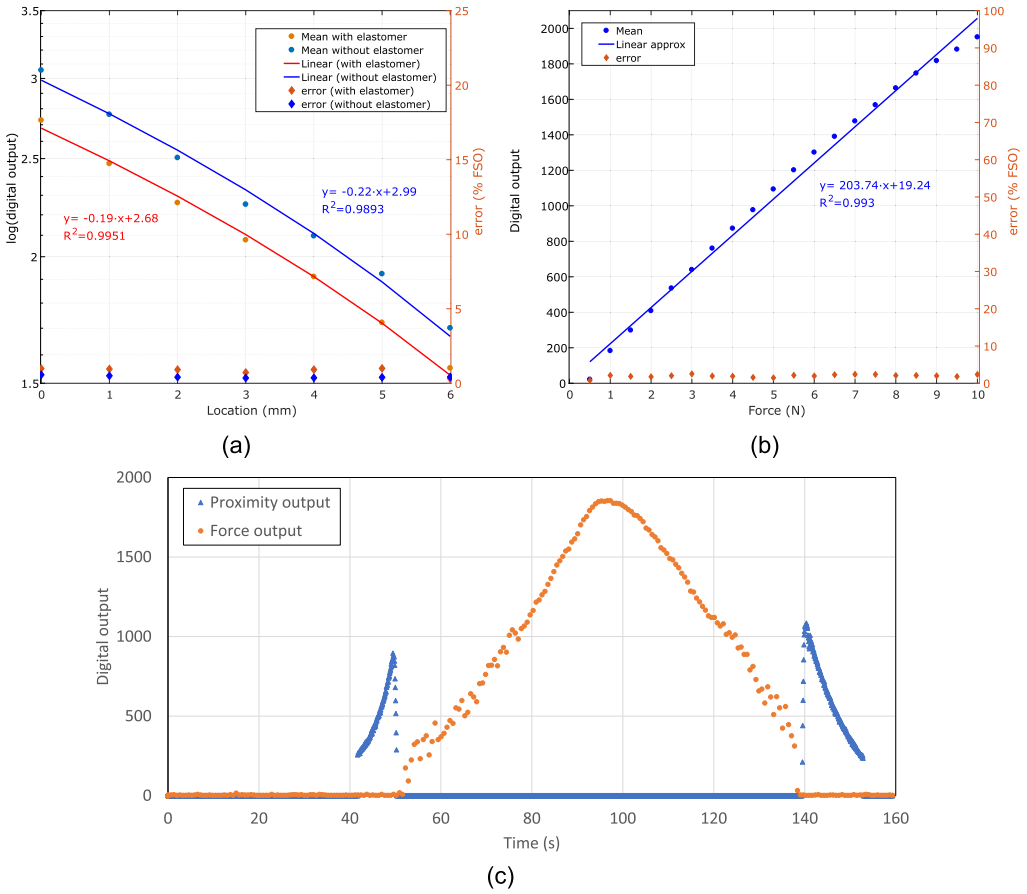

Fig. 11. (a) Proximity output of a single sensor with and without elastomer. (b) Force output of a single sensor (with elastomer). (c) Mixed experiment in which proximity and force output are shown.

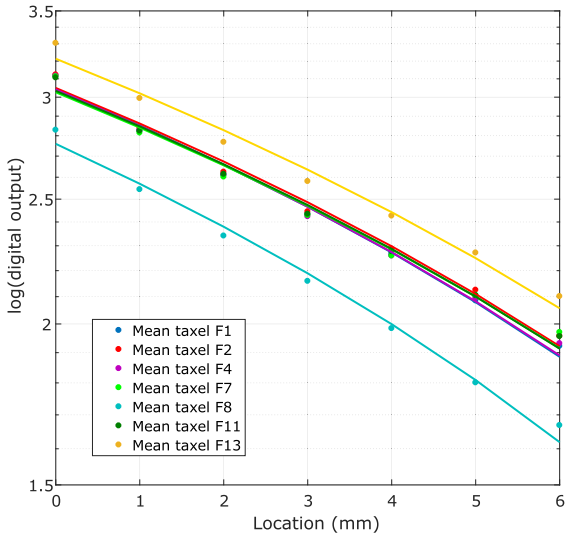

Fig. 12. Mean of the proximity output of several sensors in the array.

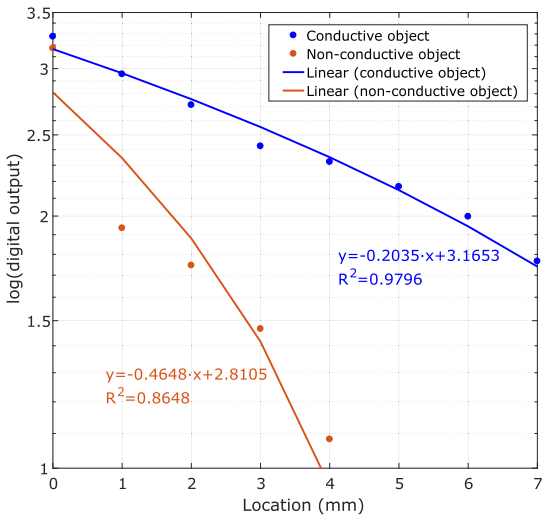

Fig. 13. Comparison between the results obtained with a metallic object and with a nonconductive object.

C. Prototype and Experimental Setup

Fig. 9 shows a picture of the prototype of proximity and tactile patch that has been realized to obtain the results of this article. In consists of an array of 4 × 4 FSRs soldered to a PCB. There are ground planes that cover both sides of the PCB. This reduces conductive and inductive interferences. Moreover, decoupling capacitors were added to reduce the effect of the inductance of the power trace. The ground planes are hatched and they are removed in the area behind the sensors to reduce parasitic capacitance.

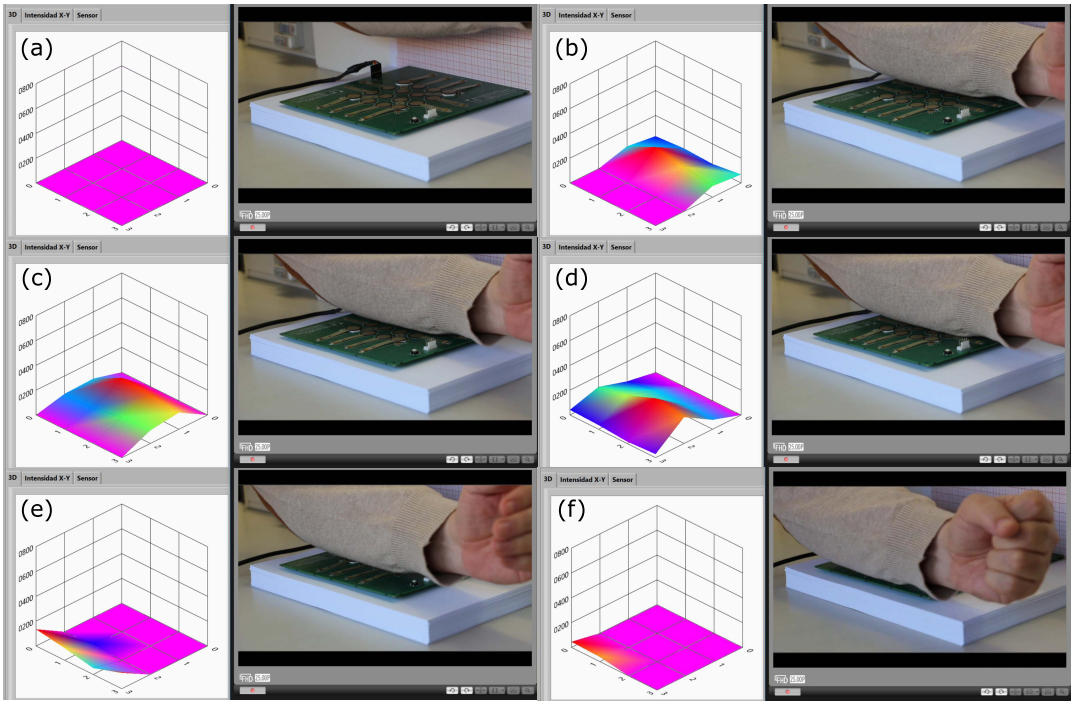

Fig. 14. Sequence of an arm displacement over the sensor.

The photograph in Fig. 9 (right) shows the back of the PCB with the PSoC. The connections have been made, as shown in Figs. 6 and 7.

In addition, Fig. 10(a) and (b) shows a picture and a diagram of the experimental setup, respectively. It is composed of a translation stage with three microstep motors. One of them (T-NA08A50 from Zaber, Vancouver, BC, Canada) controls a piston with a spring inside that exerts the force in z-axis, while the others (T-LA60A from Zaber) move the stage along the x- and y-axes. A precision force sensor (nano17 from ATI Industrial Automation, Apex, NC, USA) is placed at the end of the piston to register the force exerted against the tactile sensor. The motors and the nano17 sensor have their own control and acquisition electronics and are connected to a computer. The nano17 sensor has an aluminum prism of size 15.30 mm $\times$ 15.30 mm $\times$ 4 mm attached at the tip.

III. Results

A set of measurements were taken to observe the response of the prototype when the aluminum prism was placed at different heights with respect to the sensor surface, and with the center of its biggest side aligned with the center of the sensor under test. Fig. 11 shows the results from a single sensor in the array. Fig. 11(a) shows the digital output versus the distance when there is no contact between the metallic piece and the sensor. The test was performed with and without a 2-mm-thick elastomer on the sensor [see the onset in Fig. 10(a)]. Fifteen measurements were taken and the average as well as the error (standard deviation with respect to the full-scale output) are given. It was observed that the elastomer modifies slightly the distance range (the zero distance reference is the elastomer surface in this case), and the sensitivity and output range are smaller if the elastomer is used. This elastomer is recommended to improve the sensitivity in the force measurement [19]. Fig. 11(b) shows the response of the sensor when the contact is made between the metallic piece and the sensor, and an increasing force is exerted on it. Fifteen measurements were taken and the average as well as the error (standard deviation with respect to the full-scale output) are given. The response is almost linear, as expected for the implemented signal conditioning and the data provided in the datasheet [22]. Another test was made where the reading of both proximity and force measurements was registered as the metallic piece approached the sensor, made contact, exerted force on it, and returned to its original position following the inverse sequence [see Fig. 11(c)]. The speed of the prism is 142.88 μm/s in this test. In addition, Fig. 12 shows the output of the proximity test with the elastomer for several sensors in the array. It can be observed that the response of some of them is different in terms of sensitivity and output range. This can be due to interferences from other sensors, tracks of the PCB, sensor leads, objects in the proximity, and so on.

Fig. 13 shows a comparison between the results obtained with the metallic object of the previous experiments and those obtained with a nonconductive object. The latter is a cylinder made of polylactic acid (PLA) with a diameter of 25 mm and a height of 20 mm. It was made with a 3-D printer; the walls are 1.2 mm thick and it has an infill density of 20%. The infill density is not a key factor since the interaction is mainly with the surface of the object [17]. As expected, the response of the proposal of this article is better for conductive objects, though the PLA cylinder is detected at a distance larger than 3 mm.

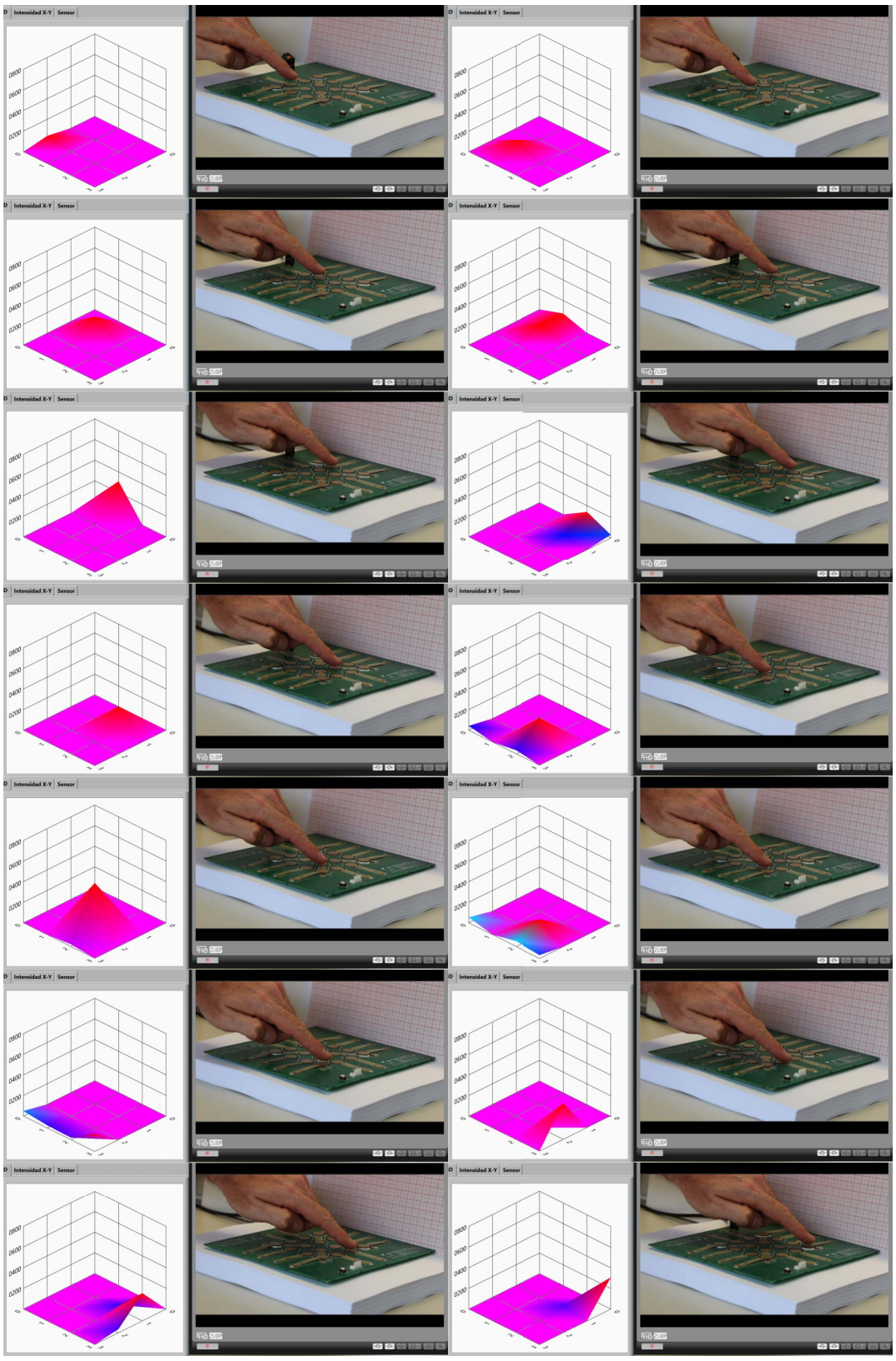

Fig. 15. Sequence of a finger displacement over the sensor.

Regarding the dynamic response, the test setup was not optimized for a high scan rate but for flexibility and the data are obtained at 20 Hz. Nevertheless, the complete scan loop for 32 proximity and tactile data was measured by means of a timer in the PSoC and it was found that it takes less than 5 ms. Therefore, the whole tactile and proximity array

TABLE II
COMPARISON OF MULTIMODAL ARTIFICIAL SKINS

Sensors	Proximity transducer /Distance range	Tactile transducer /Force range	Electronics / Scan rate	Size	Limitations	Contribution focused on	Ref.
Tactile, proximity	Custom Electrodes shared by the tactile sensor /5cm typical, 17 cm maximum	Custom Capacitive, electrodes in elastic polymer /40mN	Discrete electronics on PCB plus instrumentation /ND	22x22 mm^2 16x16 tactels 1 proximity sensor	Those derived from proximity capacitive sensing and elastomers in tactile transducers	Study of the proximity sensor, configuration of the electrodes	[17]
Tactile, proximity	Custom Capacitive coupling between two sensors /Finger sensor: 20mm typical, 40mm maximum	Custom Capacitive, elastomer layer between electrodes /tens of N @ 4cm^2 unit	Discrete electronics on PCB /ND	4 cm^2 Sensing units for large size and fingertip with 4x4 tactels and 2 proximity sensors	Those derived from proximity capacitive sensing and elastomers in tactile transducers	Full tactile and proximity suite with custom transducers and off-the shelf discrete electronic components on multi-layer PCB	[16]
Tactile, proximity	Off-the-shelf Optical Triangulation /10cm max, less than 2cm typical	Custom The same optical sensor is embedded in a transparent elastomer /5N@40mA, 2N@80mA	Based on I2C multiplexers /10Hz@8x8 array 85Hz@8 array	8 x 8 units Single optical sensor size 3.95 × 3.95 × 0.75 mm^3	Those derived from triangulation optical proximity sensing and elastomers.	Multimodal sensor based on off-the-shelf optical sensor. Characterization and performance when mounted on a gripper	[3]
Tactile, proximity, acceleration, temperature	Off-the-shelf Optical Triangulation /20cm	Custom Capacitive, metallic spring between electrodes /10N	Discrete on PCB /275us worst case delay per cell	Hexagon sensing cells 16mm side Scalable skin	Those derived from triangulation optical proximity sensing.	Multimodal scalable artificial skin and application in robot operation	[14]
Tactile, proximity, temperature	Capacitive /ND	Capacitive plus piezoresistive (polymer with carbon nanotubes) /70 kPa	ND /transducer response time 100ms capacitive sensor, 5ms piezoresistive sensor	Transducer size 1cm^2	Those derived from capacitive proximity sensing. Two force transducers required. Interference of temperature	Materials technology, fabrication techniques	[18]
Tactile, proximity	Capacitive, the electrodes of the force transducer are exploited />6mm	Off-the-shelf FSR /10N	Electronics on single chip/ Combined tactile-proximity conditioning 200Hz without communications	4 x 4 array in 10x10 cm^2	Those derived from proximity capacitive sensing. Limited distance range.	Implementing low cost proximity solution with very common off-the-shelf force sensors. Combined conditioning electronics on a single programmable chip.	This paper

can be scanned at a rate of 200 Hz without considering the communications nor other processing that the application could do in the loop.

Another simple test was performed related to the sensitivity of the proximity sensing to electromagnetic interferences (EMIs). A signal generator Rohde&Schwarz SML03S together with a $\lambda/4$ monopole antenna was used to carry out two frequency sweeps between 1 and 500 MHz at 11 dBm and between 500 and 3 GHz at 15 dBm with the antenna at 3 cm from the sensor and the metallic prism on the sensor, but without exerting any force. The standard deviation of the proximity signal in a window of 50 s did not change appreciably.

Finally, since the human body is conductive, this approach is suitable to implement applications where human–robot interaction is involved. Figs. 14 and 15 show this by showing displacements of an arm (with a sleeve) and a finger over the sensor and a set of pictures of the sensor and the arm or hand over it, together with the corresponding proximity output on the left. Fig. 14 shows the readings when an arm moves from right to left (of the picture) over the sensor. The sequence can be followed (a→b→…f in Fig. 14), and it can be observed that the sensor registers the movement of the arm. Fig. 15 shows a similar set, but now the tip of the finger is over different FSR sensors in the array. It can be observed that the output of the sensor is well localized and corresponds to the position of the finger.

IV. DISCUSSION

Table II shows the data from other reported multimodal artificial skins for comparison purposes. Proximity is commonly

based on capacitive or optical transducers. Optical transducers in these multimodal realizations are off-the-shelf devices based on triangulation. The main limitations of these sensors are the dependence of their response on the color and reflectance of the object to be detected, and they cannot detect transparent objects. They also have a minimum distance range limit and cannot detect objects below that limit. Optical sensors based on ToF have also been used to implement pretouch [12], [13]. An off-the-shelf device is used in [12]. This device has a proximity range of 100 mm with a standard deviation of 2 mm. Its main limitation is a measurement time of 15 ms and temperature interference. Another custom high-speed (measurement time below 1 ms) distance and tilt sensor based on ToF is reported in [13] with a range between 2.85 and 20 mm and 0.1-mm resolution.

The main limitation of capacitive sensors is the dependence of its response on the material of the object being detected. Moreover, the distance range is related to the size of the sensor; therefore, the performance is worse for higher spatial resolutions. In addition, they suffer from interference of electrical fields or conductive objects in the vicinity. On the other hand, their power consumption is lower than that of optical sensors. The interference of temperature on capacitive sensors is also negligible and lower than that in optical ones, since it only affects the dielectric constant of the parasitic capacitors. They also have a wide sensing region, while the optical sensors have a narrower and longer one. The use of both devices is proposed in [12] to compensate their limitations. Nevertheless, proximity sensors are not usually intended to provide accurate measurements of distance. Since the response of proximity transducers in Table II depends on the material (dielectric constant or reflectance), the sensor will register the presence of the object in the detection range but will not provide reliable information about the distance unless it is calibrated for a specific application (for instance, human–robot interaction).

Regarding force transducers in artificial skins, they are not commonly accurate sensors either. The use of elastic polymers, which is the case of most implementations in Table II, introduces nonlinearity, drift, and hysteresis, and there is a large dispersion between the force-sensing units in the array. The FSR sensor used in this article also exhibits quite large errors, such as 10% hysteresis or 2% repeatability of the same unit. Nevertheless, these sensors are widely used in many applications, particularly in robotics [19]. Since the information is often obtained from a set of force sensors, their limitations have little impact.

The size of the FSR of the developed prototype is only suitable for large tactile arrays, and therefore, the findings of this article could be used to cover large areas of a robot. Other similar multimodal proposals are based on custom patches that cover the robot body [14], [16], [17]. The distance range to a small metallic target is relatively small, though it is larger in the case of bigger conductive objects, such as human body parts. This distance is conditioned by the geometry and size of the FSR electrodes and by the spatial resolution of the array. The proposed combined solution of conditioning both sensors with a PSoC achieves a very compact solution. The scan rate is also high. This could compensate for the limited distance range in a real application, because the proximity of an object can be warned of quickly. This performance can be even enhanced if only proximity is measured before contact is established with one FSR, since the scan of the array for proximity takes 3 ms.

Finally, the application in manipulation with robotic hands and grippers is also possible, though the size of the sensor limits the spatial resolution. Nevertheless, the proposed dual conditioning with the PSoC can be extended to other off-the-shelf as well as custom sensors.

V. Conclusion

A multimodal artificial skin patch has been developed, which is able to measure force as well as proximity from a single off-the-shelf force sensor. In addition, a combined solution for proximity and force is proposed with a single programmable chip. The proximity distance range of conductive objects is above 6 mm, and the force range is 10 N. The scan rate without communications is 200 Hz. Many limitations are shared by other multimodal realizations, such as the dependence on the characteristics of the object to measure proximity or the limited accuracy of both proximity and force. However, the distance range is smaller than that of other capacitive proximity sensors because the force sensor is not custom nor designed to measure proximity. This can be compensated by the high scan rate to warn of the proximity of the object in a short time.

Since the presented patch is a demonstration prototype, there is room for improvement. First, sensors with shorter leads should be used to reduce parasitics and size. The arrangement of the sensors can also be improved to achieve a better fill factor. If the sensor is going to cover a conductive object, there should be a shield electrode in the area behind each sensor in the bottom of the PCB, and this shield should be connected to the signal "shield" (see Fig. 6). Each FSR should be placed on a flat surface, but they can be mounted on flexible or semirigid PCB to adapt to smooth surfaces. The program in the PSoC should be adapted to the specific application depending on the dynamic requirements and accuracy. Special attention has to be paid to the update of the baseline for tasks that require an object to be tracked very slowly, because the reading fades off if it is updated too often. Analog as well as digital filters can be implemented on the same chip to reduce noise. The communications of this article were not optimized for real-time operation but for testing with a personal computer and performed at 20 Hz with an RS232 serial bus. Better rates can be achieved with I2C or SPI buses that can also be implemented on the same chip. Finally, the strategy can be applied with other PSoC that is able to address more sensors and with more processing capability to add functionality and obtain a smarter patch. Other custom or off-the-shelf FSR can also be used.

References

[1] V. J. Lumelsky, M. S. Shur, and S. Wagner, "Sensitive skin," *IEEE Sensors J.*, vol. 1, no. 1, pp. 41–51, Jun. 2001.

[2] J. L. Novak and I. T. Feddema, "A capacitance-based proximity sensor for whole arm obstacle avoidance," in *Proc. IEEE Int. Conf. Robot. Automat.*, May 1992, pp. 1307–1314.
[3] R. Patel and N. Correll, "Integrated force and distance sensing using elastomer-embedded commodity proximity sensors," in *Proc. Robot., Sci. Syst.*, Ann Arbor, MI, USA, vol. 12, Jun. 2016.
[4] K. Koyama, Y. Suzuki, A. Ming, and M. Shimojo, "Integrated control of a multi-fingered hand and arm using proximity sensors on the fingertips," in *Proc. IEEE Int. Conf. Robot. Automat. (ICRA)*, May 2016, pp. 4282–4288.
[5] S. E. Navarro, M. Schonert, B. Hein, and H. Wörn, "6D proximity servoing for preshaping and haptic exploration using capacitive tactile proximity sensors," in *Proc. IEEE/RSJ Int. Conf. Intell. Robots Syst.*, Sep. 2014, pp. 7–14.
[6] B. Mayton, L. LeGrand, and J. R. Smith, "An electric field pretouch system for grasping and co-manipulation," in *Proc. IEEE Int. Conf. Robot. Automat.*, May 2010, pp. 831–838.
[7] J.-R. Tsai and P.-C. Lin, "A low-computation object grasping method by using primitive shapes and in-hand proximity sensing," in *Proc. IEEE Int. Conf. Adv. Intell. Mechatronics (AIM)*, Jul. 2017, pp. 497–502.
[8] K. Hsiao, P. Nangeroni, M. Huber, A. Saxena, and A. Y. Ng, "Reactive grasping using optical proximity sensors," in *Proc. IEEE Int. Conf. Robot. Automat.*, May 2009, pp. 2098–2105.
[9] J. Konstantinova, A. Stilli, A. Faragasso, and K. Althoefer, "Fingertip proximity sensor with realtime visual-based calibration," in *Proc. IEEE Int. Conf. Intell. Robots Syst.*, Oct. 2016, pp. 170–175.
[10] A. Maldonado, H. Alvarez, and M. Beetz, "Improving robot manipulation through fingertip perception," in *Proc. IEEE/RSJ Int. Conf. Intell. Robots Syst.*, Oct. 2012, pp. 2947–2954.
[11] K. Shimonomura, H. Nakashima, and K. Nozu, "Robotic grasp control with high-resolution combined tactile and proximity sensing," in *Proc. IEEE Int. Conf. Robot. Automat. (ICRA)*, May 2016, pp. 138–143.
[12] B. Yang, P. Lancaster, and J. R. Smith, "Pre-touch Sensing for Sequential Manipulation," in *Proc. IEEE Int. Conf. Robot. Automat. (ICRA)*, May/Jun. 2017, pp. 5088–5095.
[13] K. Koyama, M. Shimojo, T. Senoo, and M. Ishikawa, "High-speed high-precision proximity sensor for detection of tilt, distance, and contact," *IEEE Robot. Autom. Lett.*, vol. 3, no. 4, pp. 3224–3231, Oct. 2018.
[14] P. Mittendorfer, E. Yoshida, and G. Cheng, "Realizing whole-body tactile interactions with a self-organizing, multi-modal artificial skin on a humanoid robot," *Adv. Robot.*, vol. 29, no. 1, pp. 51–67, 2015.
[15] H. Yousef, M. Boukallel, and K. Althoefer, "Tactile sensing for dexterous in-hand manipulation in robotics—A review," *Sens. Actuators A, Phys.*, vol. 167, no. 2, pp. 171–187, 2011.
[16] D. Göger, H. Alagi, and H. Wörn, "Tactile proximity sensors for robotic applications," in *Proc. IEEE Int. Conf. Ind. Technol. (ICIT)*, Feb. 2013, pp. 978–983.
[17] H.-K. Lee, S.-I. Chang, and E. Yoon, "Dual-mode capacitive proximity sensor for robot application: Implementation of tactile and proximity sensing capability on a single polymer platform using shared electrodes," *IEEE Sensors J.*, vol. 9, no. 12, pp. 1748–1755, Dec. 2009.
[18] J.-O. Kim *et al.*, "Highly ordered 3D microstructure-based electronic skin capable of differentiating pressure, temperature, and proximity," *ACS Appl. Mater. Interfaces*, vol. 11, pp. 1503–1511, Dec. 2018.
[19] F. Vidal-Verdú *et al.*, "A large area tactile sensor patch based on commercial force sensors," *Sensors*, vol. 11, no. 5, pp. 5489–5507, 2011.
[20] A. Saudabayev and H. A. Varol, "Sensors for robotic hands: A survey of state of the art," *IEEE Access*, vol. 3, pp. 1765–1782, 2015.
[21] Cypress Semiconductor Corporation. *CY8C28445-24PVXI*. Accessed: Jul. 1, 2019. [Online]. Available: https://www.cypress.com/part/cy8c28445-24pvxi
[22] Interlink Electronics. (2017). *FSR Integration Guide*. Accessed: Feb. 4, 2019. [Online]. Available: http://www.produktinfo.conrad.com/datenblaetter/500000-524999/503368-an-01-en-DRUCKSENSOR_FSR_400.pdf
[23] M. Kalantari, J. Dargahi, J. Kövecses, M. G. Mardasi, and S. Nouri, "A new approach for modeling piezoresistive force sensors based on semiconductive polymer composites," *IEEE/ASME Trans. Mechatronics*, vol. 17, no. 3, pp. 572–581, Jun. 2012.
[24] J. R. Barber, "Bounds on the electrical resistance between contacting elastic rough bodies," *Proc. Roy. Soc. London. A, Math., Phys. Eng. Sci.*, vol. 459, no. 2029, pp. 53–66, 2003.
[25] L. Pastewka, N. Prodanov, B. Lorenz, M. H. Müser, M. O. Robbins, and B. N. J. Persson, "Finite-size scaling in the interfacial stiffness of rough elastic contacts," *Phys. Rev. E, Stat. Phys. Plasmas Fluids Relat. Interdiscip. Top.*, vol. 87, no. 6, Jun. 2013, Art. no. 062809.
[26] X. Hu and W. Yang, "Planar capacitive sensors–designs and applications," *Sensor Rev.*, vol. 30, no. 1, pp. 24–39, 2010.
[27] Z. Chen and R. C. Luo, "Design and implementation of capacitive proximity sensor using microelectromechanical systems technology," *IEEE Trans. Ind. Electron.*, vol. 45, no. 6, pp. 886–894, Dec. 1998.
[28] Cypress Semiconductor Corporation. (2016). *Getting Started With CapSense*. Accessed: Feb. 4, 2019. [Online]. Available: https://goo.gl/bM4sjl

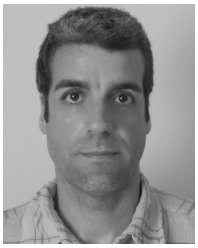

Julián Castellanos-Ramos was born in Málaga, Spain. He received the M.S. and Ph.D. degrees in industrial engineering from the Universidad de Málaga (UMA), Málaga, in 1999 and 2016, respectively.

Since 2004, he has been with the Departamento de Electrónica, UMA. He is currently a member of the Instituto de Investigación Biomédica de Málaga (IBIMA), Málaga. His current research interest includes advanced tactile sensors.

Andrés Trujillo-León was born in Córdoba, Spain, in 1984. He received the B.S. degree in telecommunication engineering, the M.S. degree in electronics engineering, and the Ph.D. degree in mechatronics engineering from the University of Málaga, Málaga, Spain, in 2008, 2011, and 2018, respectively.

He was a Research Engineer with the Departamento de Electrónica, University of Málaga, until 2014, when he enrolled in a doctoral program. He is currently a Post-Doctoral Researcher with the Institute for Intelligent Systems and Robotics (ISIR), Sorbonne University, Paris, France, where he is involved in haptics and assistive robotics. His current research interests include rehabilitation and biomedical engineering, and sensors and instrumentation.

Rafael Navas-González was born in Jaen, Spain. He received the M.Sc. degree in physics from the Universidad de Granada, Granada, Spain, in 1987, and the Ph.D. degree in microelectronics from the Universidad de Málaga (UMA), Málaga, Spain, in 2000.

Since 1993, he has been with the Departamento de Electrónica, UMA, where he is currently an Associate Professor. He is currently a member of the Instituto de Investigación Biomédica de Málaga (IBIMA), Málaga. His current research interests include advanced sensors and actuators, intelligent interfaces, and microsystems integration and their applications.

Francisco Barbero-Recio was born in Málaga, Spain, in 1987. He received the B.S. degree in industrial engineering and the M.S. degree in electronics engineering from the Universidad de Málaga (UMA), Málaga, in 2012 and 2016, respectively.

He is currently dedicated to the development of new technologies in the manufacture of polypropylene film capacitors at the TDK Group, Tokyo, Japan.

José Antonio Sánchez-Durán was born in Málaga, Spain. He received the B.S., M.S., and Ph.D. degrees in computer engineering from the Universidad de Málaga (UMA), Málaga, in 1994, 1996, and 2016, respectively.

Since 2001, he has been with the Departamento de Electrónica, UMA, where he is currently an Associate Professor. He is currently a member of the Instituto de Investigación Biomédica de Málaga (IBIMA), Málaga. His current research interests include algorithms to compensate hysteresis in tactile sensors and software development for smart tactile sensors.

Óscar Oballe-Peinado was born in Málaga, Spain. He received the B.S., M.S., and Ph.D. degrees in computer engineering from the Universidad de Málaga (UMA), Málaga, in 1993, 1999, and 2016, respectively.

Since 2000, he has been with the Departamento de Electrónica, UMA, where he is currently an Associate Professor. He is currently a member of the Instituto de Investigación Biomédica de Málaga (IBIMA), Málaga. His current research interests include application-specified integrated circuits (ASIC) and field-programmable gate arrays design, advanced tactile sensors, and tactile signal processing and applications.

Fernando Vidal-Verdú was born in Cádiz, Spain. He received the M.Sc. degree in physics from the Universidad de Seville, Seville, Spain, in 1988, and the Ph.D. degree in microelectronics from the Universidad de Málaga (UMA), Málaga, Spain, in 1996.

Since 1991, he has been with the Departamento de Electrónica, UMA, where he is currently a Full Professor. He is currently a member of the Instituto de Investigación Biomédica de Málaga (IBIMA), Málaga. He has authored or coauthored 27 international journal articles, 7 chapters of books, and more than 60 conference papers. His current research interests include smart sensors and specifically tactile interfaces.